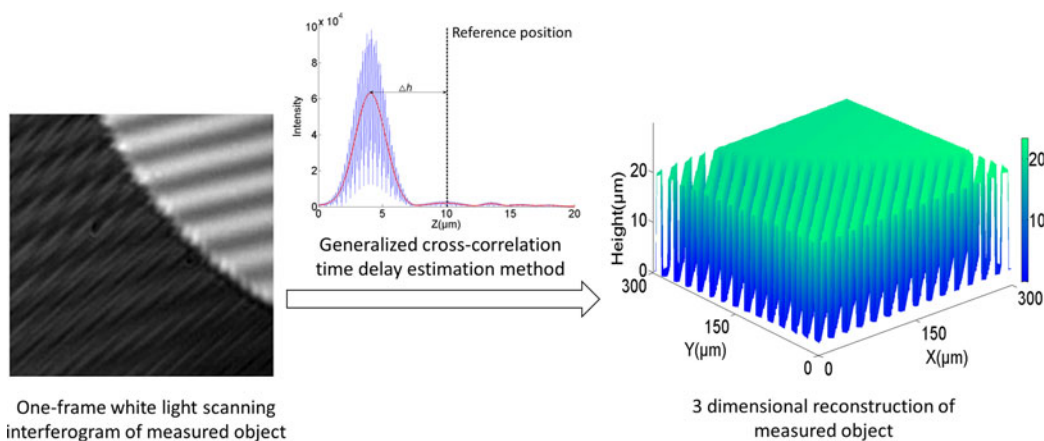# White Light Scanning Interferometry Based on Generalized Cross-Correlation Time Delay Estimation

Yunfei Zhou
Liyun Zhong
Hongzhi Cai
Jindong Tian
Dong Li
Xiaoxu Lu

One-frame white light scanning interferogram of measured object

Generalized cross-correlation time delay estimation method

3 dimensional reconstruction of measured object

White Light Scanning Interferometry Based on Generalized Cross-Correlation Time Delay Estimation

Yunfei Zhou,[1] **Liyun Zhong,**[1] **Hongzhi Cai,**[2] **Jindong Tian,**[2] **Dong Li,**[2] **and Xiaoxu Lu**[1]

[1]Guangdong Provincial Key Laboratory of Nanophotonic Functional Materials and Devices, South China Normal University, Guangzhou 510006, China
[2]College of Optoelectronic Engineering, Shenzhen University, Shenzhen 518060, China

Abstract: Based on generalized cross-correlation time delay estimation (GCTDE), a new white light scanning interferometry (WLSI) method is proposed, in which the profile information usually achieved with the zero optical path difference (ZOPD) position is replaced with the relative displacement of interference signal between different pixels. Because all spectral information of interference signal (envelope and phase) and filter is utilized, the proposed GCTDE-based WLSI method reveals the advantages of higher accuracy and better noise suppression capability. Especially, in the case where the shape of interference signal envelope is irregular, the proposed method can achieve profile measurement with high accuracy while the conventional ZOPD position locating method cannot work. Moreover, by introducing laser interferometry system to calibrate the vertical displacement of a piezoelectric ceramic transducer scanning system, the measuring accuracy of the proposed GCTDE-based WLSI is further improved. Both the simulation and the experimental results demonstrate the significant accuracy advantage of the proposed GCTDE-based WLSI.

Index Terms: Generalized cross-correlation time delay estimation, white light scanning interferometry, zero optical path difference, interference signal envelope.

1. Introduction

White light scanning interferometry (WLSI), showing large vertical measuring range (height jump) and high accuracy, has been utilized widely in various measurement, including surface roughness and profile of microscopic object [1]. Along with the development of precision manufacturing industry, profile analysis of MEMS device or semiconductor chip, possessing the height jump from a few hundred nanometers to hundreds of micron, is required [2]. As we know, atomic force microscope (AFM) is not suitable for profile measurement with large height jump due to its vertical measuring range is less than 2 μm [3]. Though laser interferometry reveals the advantages of high accuracy, non-destruction, and whole-field, its height measuring range is less than $\lambda/2$ due to phase ambiguity problem [1], [4]. To address this, WLSI is introduced, in which the surface profile information can be achieved by searching for the zero optical path difference (ZOPD) position, so its height measuring range is restricted only by the working distance of micro-objective and the scanning device.

As we know, WLSI utilizes a broadband light with short coherence length as the illumination source, so its interference fringe appears only in a small spatial region [5]. If the ZOPD between

object wave and reference wave reaches, the corresponding intensity maximum of the interference signal can be observed. That is to say, by searching for the peak position of interference signal envelope (ISE) corresponding to ZOPD position, the profile of the measured object can be constructed. Clearly, ZOPD position locating is an important research content in WLSI. To date, many ZOPD position locating methods have been reported [6]–[17], and the envelop peak detection and phase peak detection are widely utilized, in which the phase peak detection is a little bit insensitive to the envelop shape but accurate compared to the envelop peak detection with 2π ambiguity problem [6]. Chen *et al.* achieve ZOPD position through calculating the barycenter of ISE [7]. Though this method reveals rapid calculating speed, it is suitable only for the ISE function with symmetric shape. Ai *et al.* propose an improved barycenter method to achieve high accuracy ZOPD position, in which the intensity difference between interference signals is employed to determine the barycenter of ISE function [8], but its accuracy is easily affected by noise. Based on Fourier transform or Hilbert transform, Chim *et al.* perform the peak position extraction of ISE [9]–[11], but the corresponding noise suppression capability is lowered. After that, based on Fourier frequency spectrum analysis, Groot *et al.* develop a series of phase extraction of interference pattern algorithms to determine ZOPD position [12]–[14], but these algorithms need to calibrate the center wavelength of the source while they possess high accuracy. Larkin *et al.* introduce a white light phase-shifting method [15], it also reveals large error of ZOPD position locating in the case that the phase shifts is not accurate. Based on continuous wavelet transform, Sandoz *et al.* propose a peak position locating algorithm of ISE [16]. Though this algorithm shows high accuracy and good noise suppression capability, it is suitable only for the ISE with symmetric shape. By the comparison of several conventional methods, G. Gianto *et al.* find that the continuous wavelet transform (CWT) method reveals high accuracy relative to the five step phase-shifting (FSPS) and Hilbert transform (HT) methods [11], [15]–[17]. However, the accuracy of CWT method is greatly affected by the type of wavelet bases [18]. Additionally, a direct quadratic polynomial fitting ISE algorithm is presented by Park [19], but it also leads to a substantial error for the ISE with asymmetric shape. Collectively, there are various disadvantages or limitations in the above methods, ZOPD position locating with high accuracy and rapid speed is still required in WLSI.

In this study, we introduce the generalized cross-correlation time delay estimation (GCTDE) method [20]–[22] into WLSI, in which the profile information achieved by the ZOPD position locating is replaced with the relative displacement of interference signal between different pixels. Compared with the conventional HT, FSPS and CWT methods, the proposed GCTDE based WLSI method reveals the outstanding performance. Next, we will present the principle of the GCTDE based WLSI, and then give the simulation and experimental results to verify the feasibility and validity of the proposed method.

2. Fundamental Principles

In WLSI, the intensity distribution of interference pattern recorded by a digital camera can be described as [1], [4], [23]

$$I(x, y, z) = a(x, y) + b(x, y)g[z - h(x, y)] \cos \left\{ \frac{4\pi}{\lambda_0}[z - h(x, y)] \right\} + \eta \tag{1}$$

where (x, y) represents the pixel coordinate in the interference pattern, z is the vertical scanning coordinate along the optical axis; $h(x, y)$ denotes the height of measured object, $a(x, y)$, $b(x, y)$ represent the background intensity and the modulation amplitude of interference pattern, respectively; $g[z - h(x, y)]$ denotes the function of ISE, λ_0 and η are the center wavelength of white light source and the random noise in the interference pattern, respectively. For simplicity, the effect of phase offset is omitted.

In this study, by introducing GCTDE method [17] into WLSI, we can achieve ZOPD position through calculating the time delay of different pixel intensity instead of the transform of individual pixel intensity. The detailed theoretical derivation is described as following: If the intensity function of pixel (x_0, y_0) and pixel (x, y) are respectively equal to $I(x_0, y_0, z)$ and $I(x, y, z)$, by performing

Fourier transform, (1) can be rewritten as

$$\mathscr{I}(x, y, f_z) = 2\pi a(x, y)\delta(f_z) + \pi b(x, y)\exp\left[-jf_z h(x, y)\right]$$

$$\cdot\left[G\left(x, y, f_z - \frac{4\pi}{\lambda_0}\right) + G\left(x, y, f_z + \frac{4\pi}{\lambda_0}\right)\right] + \mathscr{I}_\eta(x, y, f_z)$$

$$= \mathscr{I}_0(x, y, f_z) + \mathscr{I}_+(x, y, f_z) + \mathscr{I}_-(x, y, f_z) + \mathscr{I}_\eta(x, y, f_z) \tag{2}$$

where $G(x, y, f_z)$ denotes Fourier transform spectrum of $g(z)$.

In the above Fourier transform method, ZOPD position locating is calculated through Fourier transformation of $\mathscr{I}_+(x, y, f_z)$ or $\mathscr{I}_-(x, y, f_z)$, and the envelope information of interference signal can be achieved through the inverse Fourier transformation of $\mathscr{I}_+(x, y, f_z)$ or $\mathscr{I}_-(x, y, f_z)$. That is to say, by searching for the intensity maximum of ISE, the ZOPD position can be determined [9], [10]. However, it has been reported that Fourier transform method cannot work well in the case that the noise becomes large [12]. In order to avoid the use of physical scan, Hart *et al.* introduce a Fourier transform spectroscopy method [24], in which by introducing Fourier transform spectrometer based imaging technique, the frequency spectrum information of $\mathscr{I}_+(x, y, f_z)$ or $\mathscr{I}_-(x, y, f_z)$ can be achieved directly, and then ZOPD position can be determined easily. Obviously, the measuring accuracy is nearly the same in these Fourier transform based WLSI methods. In this study, we will introduce the relative displacement of interference signal between different pixels instead of ZOPD position locating of every pixel.

If a filtering function $H(f_z)$, consisting of two center band-pass rectangle filters, is set to remove the background noise

$$\mathscr{I}(x, y, f_z)H(f_z) \approx \mathscr{I}_+(x, y, f_z) + \mathscr{I}_-(x, y, f_z) \tag{3}$$

similarly, Fourier transform of $I(x_0, y_0, z)$ can be expressed as

$$\mathscr{I}(x_0, y_0, f_z) = 2\pi a(x_0, y_0)\delta(f_z) + \pi b(x_0, y_0)\exp\left[-jf_z h(x_0, y_0)\right]$$

$$\cdot\left[G\left(x_0, y_0, f_z - \frac{4\pi}{\lambda_0}\right) + G\left(x_0, y_0, f_z + \frac{4\pi}{\lambda_0}\right)\right] + \mathscr{I}_\eta(x_0, y_0, f_z)$$

$$= \mathscr{I}_0(x_0, y_0, f_z) + \mathscr{I}_+(x_0, y_0, f_z) + \mathscr{I}_-(x_0, y_0, f_z) + \mathscr{I}_\eta(x_0, y_0, f_z) \tag{4}$$

after filtering operation with $H(f_z)$, (4) can be written as

$$\mathscr{I}(x_0, y_0, f_z)H(f_z) \approx \mathscr{I}_+(x_0, y_0, f_z) + \mathscr{I}_-(x_0, y_0, f_z) \tag{5}$$

and then performing multiplication for (3) and (5), we can achieve

$$C(f_z) = [\mathscr{I}_+(x_0, y_0, f_z) + \mathscr{I}_-(x_0, y_0, f_z)][\mathscr{I}_+(x, y, f_z) + \mathscr{I}_-(x, y, f_z)]^* \tag{6}$$

where $*$ represents the complex conjugate operation. Thus, the inverse Fourier transform of $C(f_z)$ can be expressed as

$$R(z_{f_z}) = \mathscr{I}^{-1}[C(f_z)] = \frac{1}{2\pi}\int_{-\infty}^{+\infty} C(f_z)\exp\left(j2\pi f_z \cdot z_{f_z}\right)df_z \tag{7}$$

According to GCTDE method, when $R(z_{f_z})$ reaches the maximum, z_{f_z} is equal to the relative displacement of interference signal between pixel (x_0, y_0) and pixel (x, y).

$$R(z_{f_z}) \approx \left(b(x_0, y_0)g[z - h(x_0, y_0)]cos\left\{\frac{4\pi}{\lambda_0}[z - h(x_0, y_0)]\right\}\right)$$

$$\otimes\left(b(x, y)g[-z - h(x, y)]cos\left\{\frac{4\pi}{\lambda_0}[-z - h(x, y)]\right\}\right) \tag{8}$$
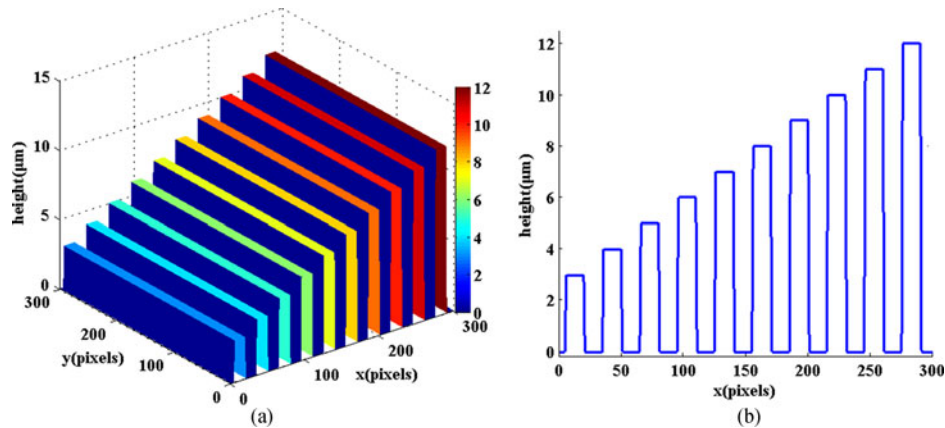
Fig. 1. (a) Profile of the simulated step. (b) The corresponding cross section distribution of (a).

where $\otimes$ represents the convolution operation; $h(x_0, y_0)$ and $h(x, y)$ denote the heights of pixel (x_0, y_0) and pixel (x, y), respectively. Assuming $\Delta h = h(x, y) - h(x_0, y_0)$, (8) can be rewritten as

$$R(z_{f_z}) \approx b(x_0, y_0)b(x, y) \int_{-\infty}^{+\infty} g[z - h(x_0, y_0)] \cos\left\{\frac{4\pi}{\lambda_0}[z - h(x_0, y_0)]\right\} \cdot g[z - h(x_0, y_0) + (z_{f_z} - \Delta h)]$$

$$\cdot \cos\left\{\frac{4\pi}{\lambda_0}[z - h(x_0, y_0) + (z_{f_z} - \Delta h)]\right\} dz \qquad (9)$$

From (9), we can see that if $z_{f_z} - \Delta h = 0$, $R(z_{f_z})$ can reach its maximum. Clearly, this result exhibits that the proposed GCTDE method is suitable for the ISE function not only Gaussian shape, but also the asymmetric shape or multi-peak shape.

As described above, in Fourier transform method, ZOPD position can be achieved with the inverse Fourier transform of $\mathscr{I}_+(x, y, f_z)$ [9], [10], in which only the envelope information of interference signal is employed. However, using the GCTDE method, all spectral information of interference signal, including the envelope and the phase, are utilized, so its measuring accuracy will be greatly improved.

3. Numerical Simulation

Numerical simulation is employed to verify the validity of the proposed GCTDE method. The simulated object is one reflective step, containing ten different step-heights in the range of 3–12 μm and the same distance between adjacent steps. The size of fringe pattern is 300 × 300 pixels (-1.5 mm $\leq x, y \leq 1.5$ mm). Fig. 1(a) and (b) present the surface profile of the simulated object and the corresponding cross section distribution.

According to (1), the background intensity, modulation amplitude and center wavelength of white light source are set as $a = 90$, $b = 80$, $\lambda_0 = 0.7$ μm, respectively. For convenience, we set the ISE function as $g[z - h(x, y)] = \exp\{-[z - h(x, y)/l_c]^2\}$, in which the coherence length of white light source is $l_c = \lambda_0^2/\Delta\lambda$, and the spectral bandwidth is $\Delta\lambda = 0.4$ μm. In addition, the random noise with 3% of background intensity is added to the interference pattern; the scanning interval is set as 0.05 μm and its scanning is in the range of 0 μm to 20 μm.

Fig. 2 illustrates the calculating process of the GCTDE proposed method. First, as shown in Fig. 2(a) and (c), the intensity distributions of two interference signals in the reference pixel (100, 100) and the measured pixel (285, 285) are chosen as $I(x_0, y_0, z)$ and $I(x, y, z)$, respectively. Second, we implement two interference signals with Fourier transform and filtering operation, as shown Fig. 2(b) and (d), in which the red rectangular squares denote the filtering function $H(f_z)$. Third, we perform the multiplication for Fig. 2(b) and the complex conjugate of Fig. 2(d), and then the inverse Fourier transform, the achieved result is presented as the blue curve of Fig. 2(e). Fourth,
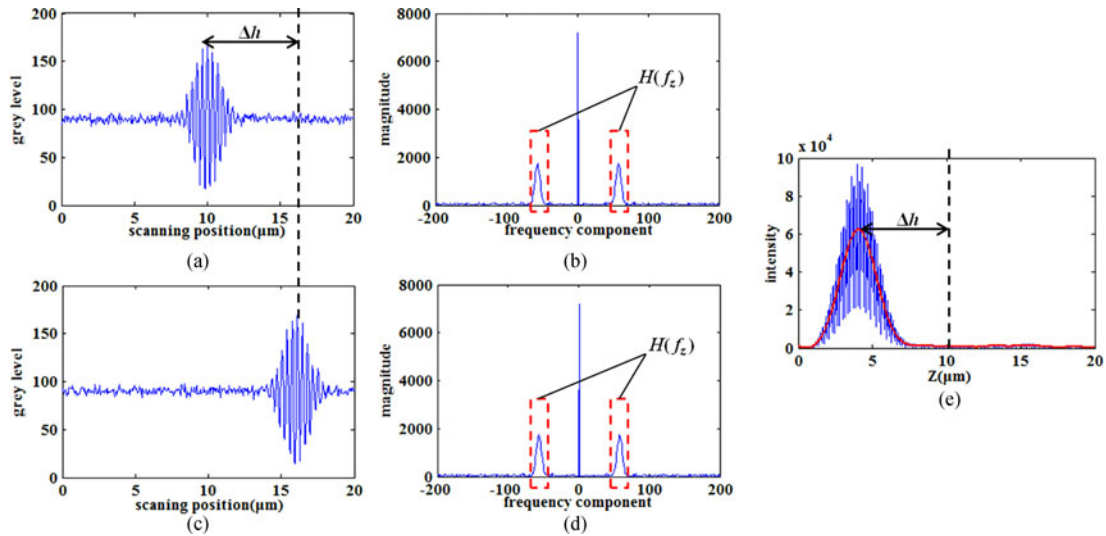
Fig. 2. (a) Intensity distribution of simulated interference signal $I(x_0, y_0, z)$. (b) Result of (a) implemented with Fourier transform and filtering operation. (c) Intensity distribution of simulated interference signal $I(x, y, z)$. (d) Result of (c) implemented with Fourier transform and filtering operation. (e) Blue curve achieved by the multiplication for (b) and the complex conjugate of (d), and then the inverse Fourier transform; red curve achieved by the low-pass filtering for blue curve.
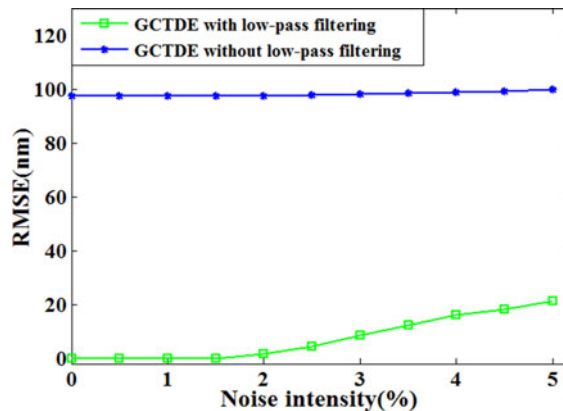

Fig. 3. Variation curves of RMSEs of the achieved height with the proposed GCTDE method with and without low-pass filtering in different noise level, respectively.

by low-pass filtering (Butterworth based zero-phase filtering) for the blue curve of Fig. 2(e), we can achieve the corresponding red curve. Finally, by searching for the maximum of the red curve of Fig. 2(e), the relative displacement △h of interference signal between the measured pixel (285, 285) and the reference pixel (100, 100) can be achieved, as shown in Fig. 2(e). Subsequently, based on the pixel-by-pixel relative displacement calculation, we can achieve the relative height of the measured object.

Next, we use the numerical simulation to present the influence of low-pass filtering on the measuring accuracy. By changing the noise level, Fig. 3 shows the corresponding root mean square errors (RMSEs) of the difference between the preset value and the height achieved with the proposed GCTDE method without and with low-pass filtering, respectively. From Fig. 3, we can see that using the proposed GCTDE method, the measuring accuracy with low-pass filtering is significantly better than without low-pass filtering. Therefore, in the following study, the GCTDE method with low-pass filtering is employed for numerical simulation and experimental research.
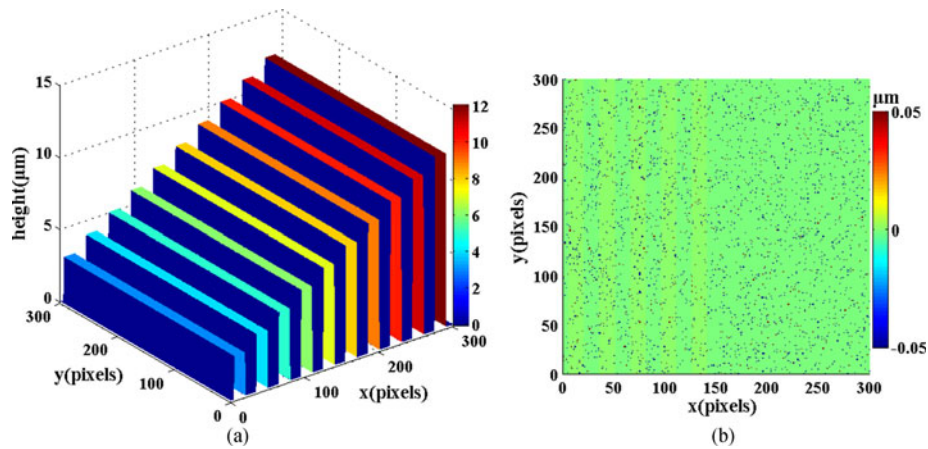
Fig. 4. (a) Profile of stimulated step achieved with the proposed GCTDE method. (b) The height difference between the preset value and (a).
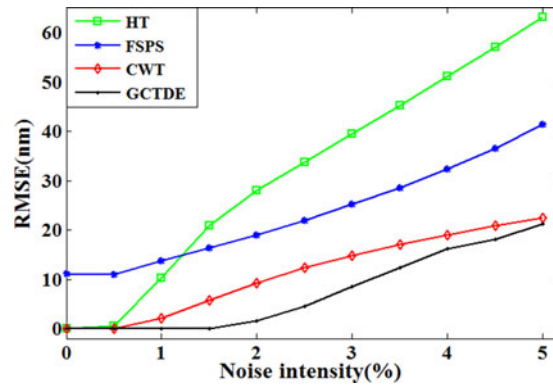

Fig. 5. Variation curves of RMSEs of the achieved height with different methods in different noise level.

Based on the proposed GCTDE method, Fig. 4(a) presents the profile of measured object, and Fig. 4(b) gives the difference between the preset value and the achieved height.

For comparison, we also give the profiles achieved with HT, FSPS and CWT methods, respectively. It is found that the root mean square error (RMSE) of the difference between the preset value and the height achieved with above four methods are respectively 39.5 nm (HT), 25.2 nm (FSPS), 14.8 nm (CWT) and 8.5 nm (GCTDE), indicating that the accuracy of profile measurement with the proposed GCTDE method is significantly higher than other three methods. Moreover, by changing the noise level, we also give the corresponding RMSEs achieved with HT, FSPS, CWT and GCTDE methods, respectively, as shown in Fig. 5. It is observed that though RMSEs with all above methods are increased with noise level, but the proposed GCTDE method reveals the better noise suppression capability.

4. Experimental Results and Discussion

As shown in Fig. 6, a vertical WLSI system (Linnik type), consisting of light source, white light interference system, laser interference calibration system, image recording system, and image processing system, is built up to verify further the proposed GCTDE method.

A Halogen lamp (NARVA, HLL12V50W) is employed as the white light source. A measured MEMS device (MEMSCAP.OA MEM103) is mounted on a piezoelectric ceramic transducer (PZT) displacement stage (NewPi, Model: XP-612.XY80S and XE-501 controller), which is chosen to achieve the vertical scanning. The interference pattern of WLSI is achieved with the ZOPD position
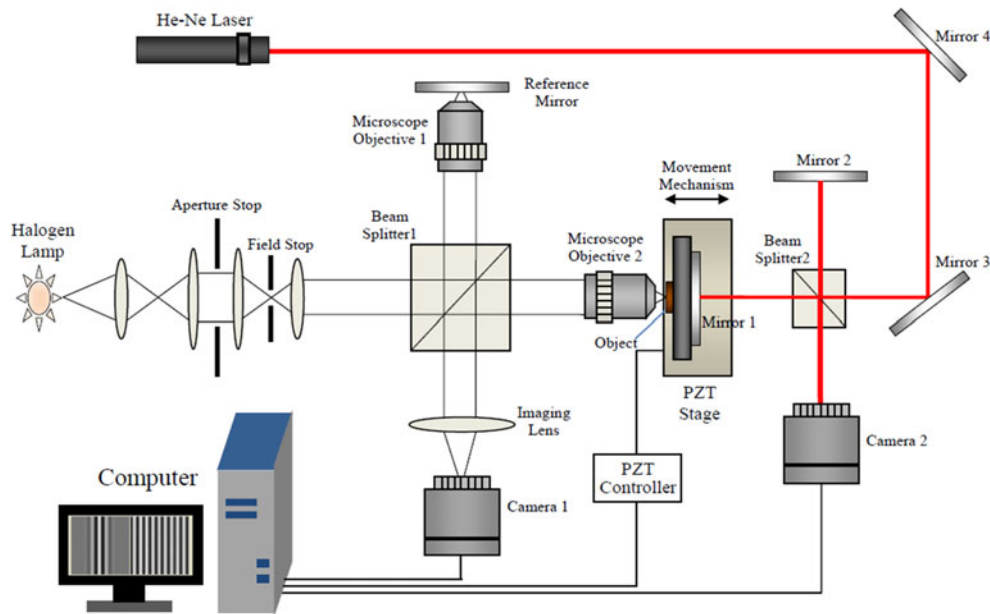
Fig. 6. Schematic of WLSI experimental system. PZT, piezoelectric ceramic transducer.

locating method. As we know, to improve the measuring accuracy, the displacement of PZT device needs to be calibrated. In this study, we introduce a laser interference system to calibrate the vertical scanning displacement of PZT device, in which a standard flat mirror 1 is fixed on the measured object platform, so the movement of the measured object is same with mirror 1. When PZT device moves a step-interval, camera 1 and camera 2 (CMOS, Model: HV1303UM.) simultaneously capture the corresponding interference patterns, respectively. White light interference pattern captured by camera 1 is employed for profile measurement of the object, and laser interference pattern captured by camera 2 is utilized for phase shifts extraction, achieving the calibration of PZT displacement.

Also, in our experimental system, the magnifications of micro-objective 1 and micro-objective 2 are equal to $10\times$; the nominal value of grid height in MEMS device is 20 μm, and the step-interval of PZT moving is set as 60 nm. Fig. 7(a) shows a microscopic image of measured MEMS device, and Fig. 7(b) gives the magnification of white rectangular square in Fig. 7(a) with a size of 560 μm $\times$ 420 μm (400 $\times$ 300 pixels) captured by camera 1 without interference. Fig. 7(c) and (d) present two interference patterns of WLSI captured by camera 1 in two different PZT scanning positions, respectively.

Fig. 8(a) and (c) show the intensity distributions of two experimental interference signals with asymmetric shape, respectively. In this situation, using the conventional ZOPD position locating method, it is very difficult to achieve the accurate profile of measured object [15], [16], [19]. To address this, we employ the proposed GCTDE method to perform the profile measurement of MEMS device. Like the numerical simulation, we first choose the intensity distributions of two interference signals of the measured pixel (400, 1) and the reference pixel (1, 300) as $I(x, y, z)$ and $I(x_0, y_0, z)$, as shown in Fig. 8(a) and (c), respectively. Fig. 8(b) and (d) present the corresponding results implemented with Fourier transform and filtering operation. Fig. 8(e) gives the relative displacement Δh of interference signal between the measured pixel (400, 1) and the reference pixel. Finally, based on the pixel-by-pixel relative displacement calculation, the relative height of measured object can be achieved, as shown in Fig. 9. It is found that the grid height of MEMS device achieved with the proposed GCTDE method (19.766 μm) is greatly consistent with the nominal value of 20 μm.

Moreover, to compare the measuring accuracy of WLSI system and laser interferometry system, we employ a wedge-shaped mirror with a 2 μm height as the measured object, in which the step-interval of PZT moving is set to 20 nm. As shown in Fig. 10(a)–(d), two interference patterns
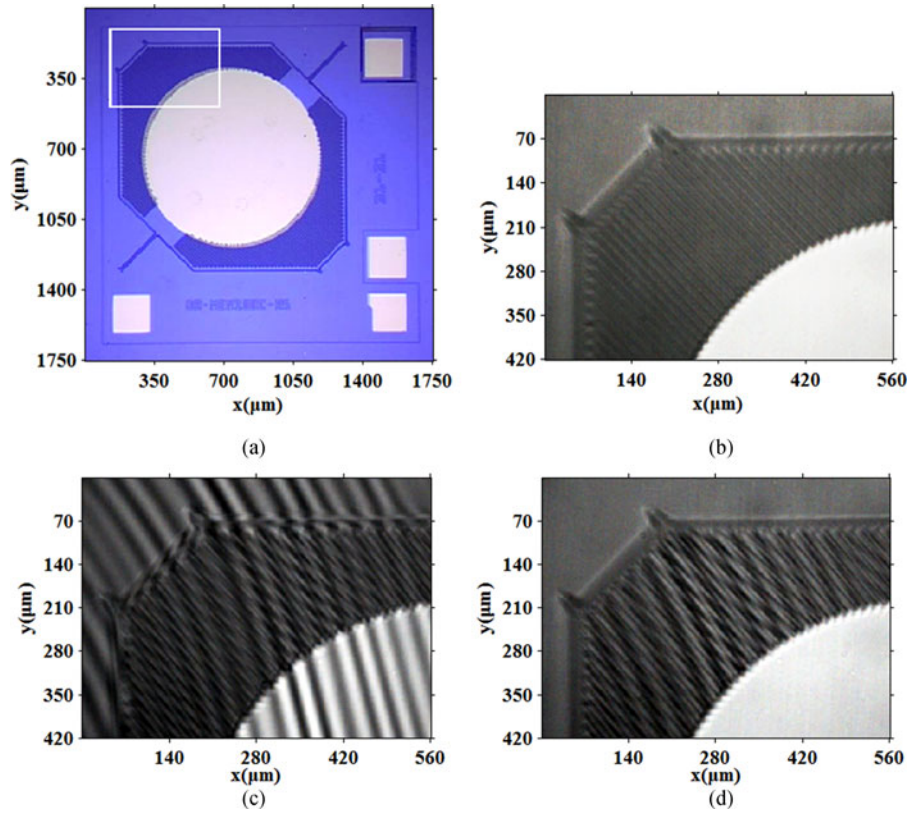
Fig. 7. (a) Microscopic image of the measured MEMS device. (b) The magnification of white rectangular square in (a) without interference. (c) and (d) Two interference patterns of WLSI captured in two different PZT scanning positions.
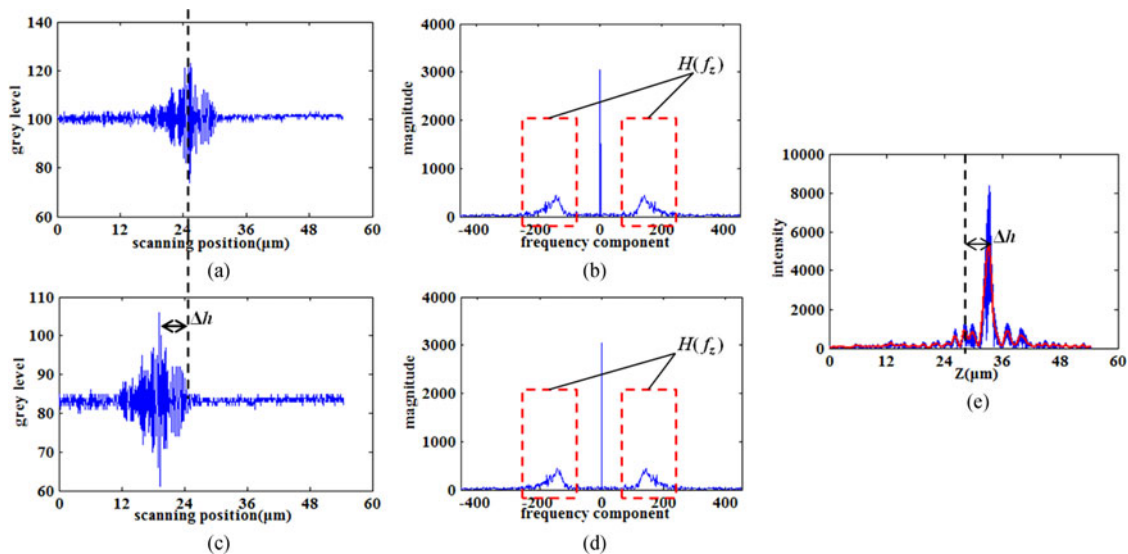

Fig. 8. (a) Intensity distribution of experimental interference signal $I(x_0, y_0, z)$. (b) Result of (a) implemented with Fourier transform and filtering operation. (c) Intensity distribution of experimental interference signal $I(x, y, z)$. (d) Result of (c) implemented with Fourier transform and filtering operation. (e) Blue curve achieved with the multiplication for (b) and the complex conjugate of (d), and then the inverse Fourier transform; red curve achieved by the low-pass filtering for blue curve.
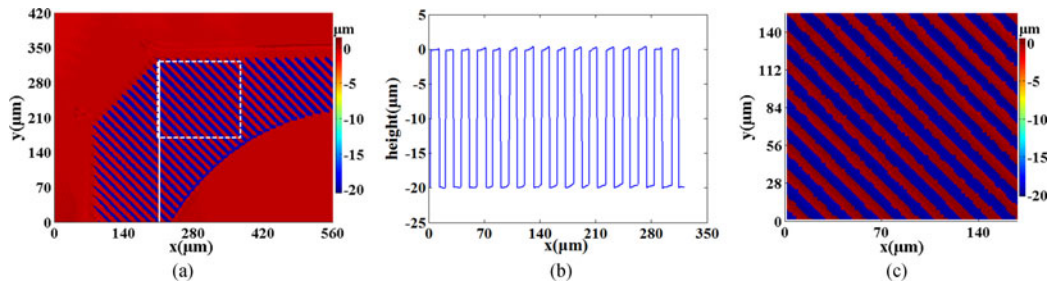
Fig. 9. (a) Profile of MEMS device achieved with the proposed GCTDE method. (b) The height distribution marked with the white line in (a). (c) Profile marked with the dashed square in (a).
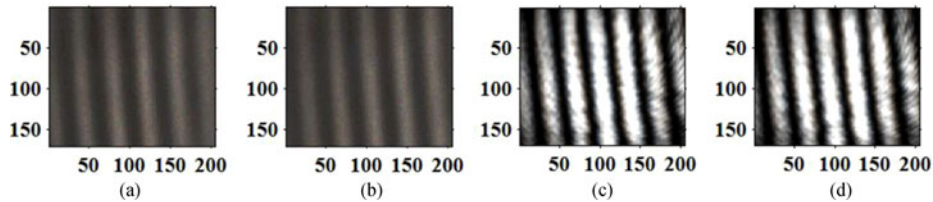

Fig. 10. (a) and (b) Two interference patterns captured with WLSI system. (c) and (d) Two interferograms captured with laser interferometry system.
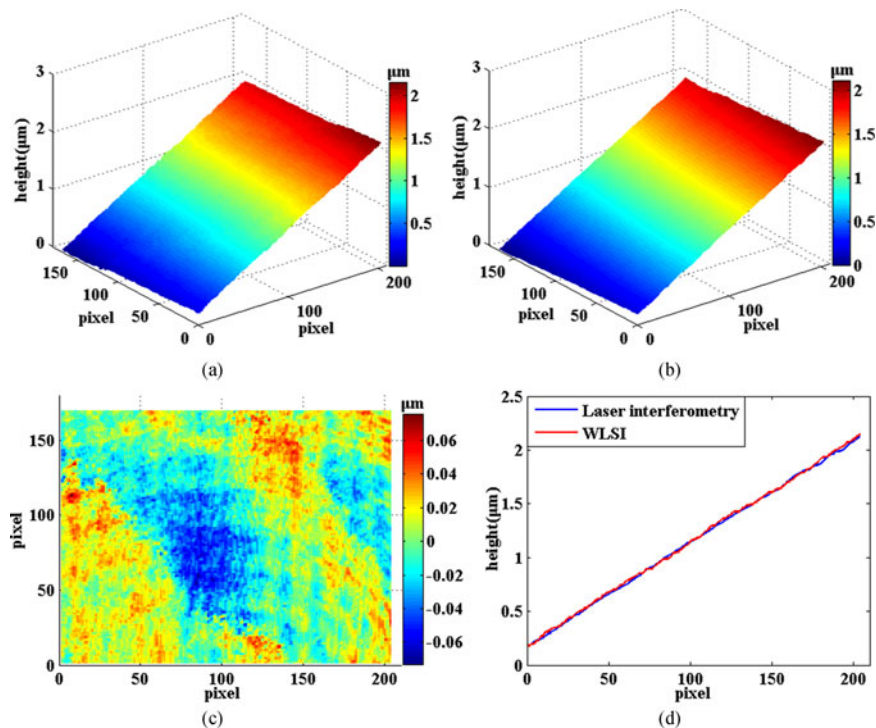

Fig. 11. (a) Profiles of a mirror achieved with the proposed GCTDE based WLSI. (b) Profiles of a mirror achieved with laser interferometry. (c) The height difference between (a) and (b). (d) Height distribution of the first column in (a) and (b).

captured by WLSI system and two interferograms captured by laser interferometry are presented, respectively. Fig. 11(a)–(d) show the profiles achieved with the proposed GCTDE method and laser interferometry method. It is found that the average height difference of mirror achieved with above two interferometry methods is less than 22 nm, and the deviation between the nominal value and the height achieved with laser interferometry method or the proposed GCTDE method is only 1%. This
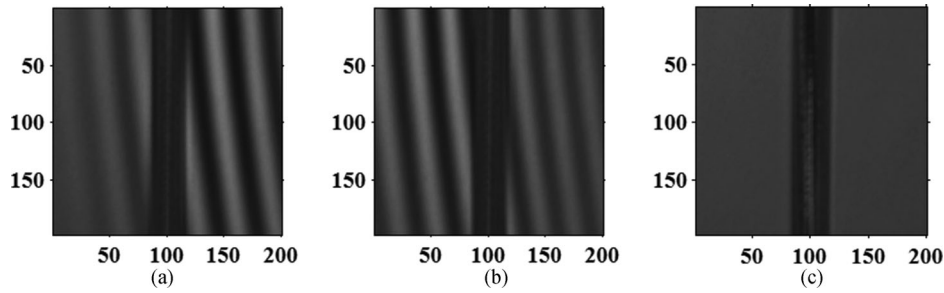
Fig. 12. Three interference patterns in WLSI captured in three different PZT scanning positions.
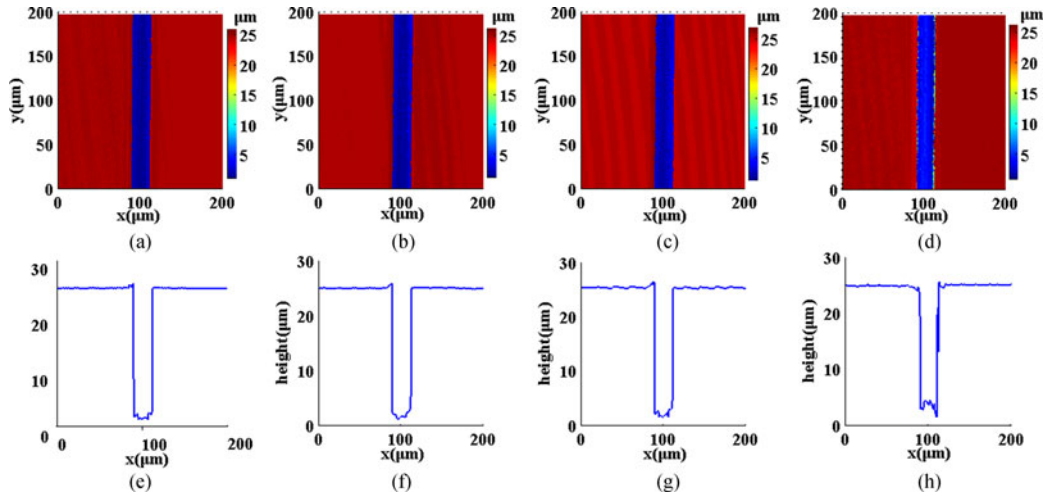

Fig. 13. (a)–(d) The profiles achieved with the proposed GCTDE method, CWT, HT, FSPS methods, respectively. (e)–(h) The height distribution of the first column in (a)–(d), respectively.

result demonstrates that the accuracy of profile measurement with the proposed GCTDE method is nearly the same with high accuracy laser interferometry.

Furthermore, to perform the experimental comparison about the accuracy and noise suppression capability between the proposed GCTDE method and other conventional methods, we employ a semiconductor chip (optical wavelength selective switch) as the measured object. The magnifications of micro-objective 1 and micro-objective 2 are equal to 10×, and the step-interval of PZT moving is set as 40 nm. Fig. 12 presents three interference patterns of WLSI captured by camera 1 in three different PZT scanning positions, respectively. The profiles achieved with the proposed GCTDE method, CWT, HT and FSPS methods are shown in Fig. 13(a)–(d), and the corresponding height distribution of the first column in Fig. 13(a)–(d) are given in Fig. 13(e)–(h), respectively. Clearly, these experimental results present that the accuracy of profile measurement with the proposed GCTDE method is higher than HT and FSPS methods and similar with the CWT method, which are consistent with the numerical simulation work. Though the result achieved with CWT method shows high accuracy and good noise suppression capability, but it is suitable only for the ISE function with symmetric shape. However, in addition to maintaining high accuracy, the proposed GCTDE method can work well in the case that the shape of ISE function is irregular, and this will greatly expand the application of WLSI.

5. Conclusion

In this study, a GCTDE based WLSI method is proposed, in which the profile information achieved with the conventional ZOPD position locating method is replaced with the relative displacement of

interference signal between different pixels. Compared with the ZOPD position locating based WLSI (HT, CWT and FSPS) methods, due to all spectral information of interference signal (envelope and phase) and filters are utilized, the proposed GCTDE based WLSI method reveals the advantages of higher accuracy and better noise suppression capability. Especially, in the case that the shape of ISE function is irregular, the proposed GCTDE based WLSI can achieve profile measurement with high accuracy while the ZOPD position locating method cannot work. In addition, by introducing laser interferometry system into WLSI, the displacement of PZT scanning system can be calibrated conveniently, and then the measuring accuracy of WLSI system is further improved. In a word, combining above WLSI system and the proposed GCTDE method, we can achieve high accuracy profile measurement with large height jump. Both the simulation and the experimental results demonstrate the significant accuracy advantage of the proposed GCTDE method, and this will greatly expand the application of WLSI.

References

[1] F. Salzenstein, P. Montgomery, and A. Boudraa, "Local frequency and envelope estimation by Teager-Kaiser energy operators in white-light scanning interferometry," *Opt. Exp.*, vol. 22, no. 15, pp. 18325–18334, 2014.

[2] P. Pavlicek and V. Michalek, "White-light interferometry—Envelope detection by Hilbert transform and influence of noise," *Opt. Lasers Eng.*, vol. 50, no. 8, pp. 1063–1068, 2012.

[3] C. O'Mahony, M. Hill, M. Brunet, R. Duane, and A. Mathewson, "Characterization of micromechanical structures using white-light interferometry," *Meas. Sci. Technol.*, vol. 14, no. 10, pp. 1807–1814, 2003.

[4] S. Ma, C. Quan, R. Zhu, C. Tay, L. Chen, and Z. Gao, "Micro-profile measurement based on windowed Fourier transform in white-light scanning interferometry," *Opt. Commun.*, vol. 284, nos. 10–11, pp. 2488–2493, 2011.

[5] J. T. Dong and R. S. Lu, "A five-point stencil based algorithm used for phase shifting low-coherence interference microscopy," *Opt. Lasers Eng.*, vol. 50, no. 3, pp. 502–511, 2012.

[6] A. Harasaki, J. Schmit, and J. C. Wyant, "Improved vertical-scanning interferometry," *Appl. Opt.*, vol. 39, no. 13, pp. 2107–2115, May 2000.

[7] S. Chen, A. Palmer, K. Grattan, and B. Meggitt, "Digital signal-processing techniques for electronically scanned optical-fiber white-light interferometry," *Appl. Opt.*, vol. 31, no. 28, pp. 6003–6010, 1992.

[8] C. Ai and E. L. Novak, "Centroid approach for estimating modulation peak in broad-bandwidth interferometry," U.S. Patent 5 633 715, 1997.

[9] G. S. Kino and S. S. Chim, "Mirau correlation microscope," *Appl. Opt.*, vol. 29, no. 26, pp. 3775–3783, 1990.

[10] S. S. Chim and G. S. Kino, "Correlation microscope," *Opt. Lett.*, vol. 15, no. 10, pp. 579–581, 1990.

[11] S. S. Chim and G. S. Kino, "Three-dimensional image realization in interference microscopy," *Appl. Opt.*, vol. 31, no. 14, pp. 2550–2553, 1992.

[12] P. de Groot and L. Deck, "Surface profiling by analysis of white-light interferograms in the spatial frequency domain," *J. Modern Opt.*, vol. 42, no. 2, pp. 389–401, 1995.

[13] P. de Groot, X. C. de Lega, J. Kramer, and M. Turzhitsky, "Determination of fringe order in white-light interference microscopy," *Appl. Opt.*, vol. 41, no. 22, pp. 4571–4578, 2002.

[14] P. de Groot and X. C. de Lega, "Signal modeling for low-coherence height-scanning interference microscopy," *Appl. Opt.*, vol. 43, no. 25, pp. 4821–4830, 2004.

[15] K. G. Larkin, "Efficient nonlinear algorithm for envelope detection in white light interferometry," *J. Opt. Soc. Amer. A—Opt. Image Sci. Vision*, vol. 13, no. 4, pp. 832–843, 1996.

[16] P. Sandoz, "Wavelet transform as a processing tool in white-light interferometry," *Opt. Lett.*, vol. 22, no. 14, pp. 1065–1067, 1997.

[17] G. Gianto, F. Salzenstein, and P. Montgomery, "Comparison of envelope detection techniques in coherence scanning interferometry," *Appl. Opt.*, vol. 55, no. 24, pp. 6763–6774, Aug. 2016.

[18] A. Mojsilovic, M. V. Popovic, and D. M. Rackov, "On the selection of an optimal wavelet basis for texture characterization," *IEEE Trans. Image Process.*, vol. 9, no. 12, pp. 2043–2050, Dec. 2000.

[19] M. C. Park and S. W. Kim, "Direct quadratic polynomial fitting for fringe peak detection of white light scanning interferograms," *Opt. Eng.*, vol. 39, no. 4, pp. 952–959, 2000.

[20] C. H. Knapp and G. C. Carter, "The generalized correlation method for estimation of time delay," *IEEE Trans. Acoust. Speech Signal Process.*, vol. ASSP-24, no. 4, pp. 320–327, Aug. 1976.

[21] M. Azaria and D. Hertz, "Time delay estimation by generalized cross correlation methods," *IEEE Trans. Acoust. Speech Signal Process.*, vol. ASSP-32, no. 2, pp. 280–285, Apr. 1984.

[22] D. Hertz and M. Azaria, "Time delay estimation between two phase shifted signals via generalized cross-correlation methods," *Signal Process.*, vol. 8, no. 2, pp. 235–257, 1985.

[23] R. J. Recknagel and G. Notni, "Analysis of white light interferograms using wavelet methods," *Opt. Commun.*, vol. 148, nos. 1–3, pp. 122–128, 1998.

[24] M. Hart, D. G. Vass, and M. L. Begbie, "Fast surface profiling by spectral analysis of white-light interferograms with Fourier transform spectroscopy," *Appl. Opt.*, vol. 37, no. 10, pp. 1764–1769, 1998.